F. Summary of the Methods for Producing Large Plasma Membrane Fragments and Avoiding Excessive Fragmentation of Replicas

The following methodological precautions and improvements will help to reproducibly produce large plasma membrane fragments and replicas without excessive fragmentation. Although individually these are minor modifications, but collectively they exert a substantial impact.

1. Employ an alcian-blue coat, rather than a poly-L-lysine coat (Rutter *et al.*, 1988; Sanan and Anderson, 1991).

2. In the protocol to observe the top membrane, before overlaying the alcian-blue-coated coverslips, remove the excess water from the specimen, leaving just enough buffer to cover the cell.

3. To cleave off the upper membrane attached to the overlaid coverslip, float the coverslip off very gently by adding cleavage medium (using the surface tension of the buffer to float the coverslip). If this is not done gently enough, the membrane will be fragmented.

4. Shave off the frozen sample with a glass or diamond knife, with the angle between the knife and the cover glass adjusted to a shallow angle (less than 6°), so that most of the excess water and the cytoplasm are removed and the cytoplasmic surface of the cell membrane could be exposed after light etching. Since replicas with too many variations in height tend to break when they are removed from the coverslip and placed on the water surface, removal of the excess cytoplasm helps to avoid replica breakage.

5. Apply collodion immediately after the replicas are removed from the cold chamber (before the replicas are removed from the coverslip on the water surface), to fortify the replica. This step helps to prevent replica breakage when the replicas are removed from the cover slip. Dissolve away the collodion coat in *n*-pentyl acetate, after the large replicas are successfully removed from the glass surface.

6. Use a solution of 1% hydrofluoric acid to slightly dissolve the glass surface, to facilitate the removal of the replicas from the cover slip.

7. To keep as many colloidal gold particles attached on the platinum replicas as possible, include 0.5–1% Kodak Photo-Flo 200 in all of the solutions used to remove the replicas from the coverslips.

G. Creation of Stereo Views (Anaglyphs)

The term "anaglyph" refers to any image that has the appearance of being raised from the surface of the paper. For the stereo views (anaglyphs), image pairs have to be obtained by tilting the stage at ±12.5° from the vertical axis. For details on the production of anaglyphs, see Heuser (2000).

H. 3-D Reconstruction of the MSK by Electron Tomography

In X-ray tomography, an increasingly popular technology for disease diagnosis, X-rays irradiate the body at various angles, and from the X-ray images taken at various rotated or tilted images, sliced images of the body are calculated for reconstructing the 3-D images of the body. In electron tomography, the specimen stage is tilted with respect to the incident electron beam in the transmission electron microscope. The mathematical formulation is basically the same, except that the tilt angle may be limited within $\pm\sim 70^\circ$, limiting the z-resolution. In addition, since the axis of rotation slightly shifts around upon stage tilting, inducing large shifts in the location of the observed detailed structures (large as compared to the subnanometer size of the object we observe under the electron microscope), correction to compensate for this effect is needed for three-dimensional reconstruction. Usually, EM images are taken every 1°, and therefore, for the tilt angles between ±70°, 141 tilt images are taken for a single view field (Fig. 4).

Such quantitative data acquisition and three-dimensional image reconstruction in EM were developed and automated in the 1990s, resulting in the current prevalence of this method. Four key features in the development were: (1) the development of the tilting stage that allows accurate rotation; (2) the development of an electron microscope with z-axis correction and a side-entry specimen holder; (3) the development of a scientific CCD camera with high sensitivity, resolution (1024 × 1024 pixels or more, with a pixel size of 0.85 nm or better on the sample, which should be finer than the platinum grain size), and linearity; (4) the creation of software for the automatic data acquisition of a series of tilted images (Medalia *et al.*, 2002). Recently, this method has increasingly been used to determine molecular forms as well as cellular structures (Lucic *et al.*, 2005).

We generally use the "IMOD" software package, created by Dr. J. R. McIntosh of the University of Colorado at Boulder (Kremer *et al.*, 1996), running on Linux,

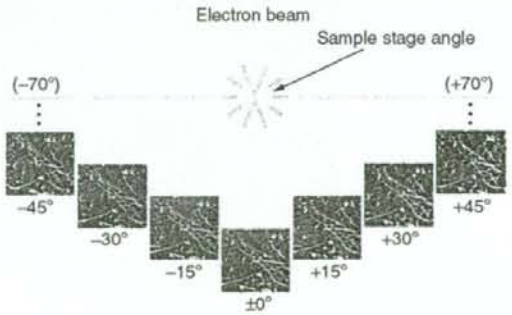

Fig. 4 EM images obtained at different tilt angles of the specimen stage with respect to the incident electron beam. Reproduced from Morone *et al.* (2006). © 2003 The Rockfeller University Press.

for the generation of a series of sliced images (for example, about 100 image sections of every 0.8–1.3 nm) from a series of tilted images. Corrections for the tilt and the long-wavelength undulations of the membrane can also be achieved with the IMOD software. 3D rendering (displaying 3D images in different ways) can be carried out using the Templace Graphics AMIRA software package, operating on a Linux system.

III. 3D Structure of the Cytoskeleton-Plasma Membrane Interface

A. The Cytoplasmic Surface of the Plasma Membrane of Cultured Cells is Entirely Coated with the Meshwork of the Actin-Based MSK

A typical electron micrograph, providing a bird's-eye view of the cytoplasmic surface of a large area of the upper cell membrane of a cultured normal rat kidney (NRK) cell line, is shown in Fig. 5. A number of such EM images showing the cytoplasmic surfaces of large cell membrane fragments were obtained for NRK and fetal rat skin keratinocyte (FRSK) cells, suggesting that the entire (upper) plasma membrane, except for the places where clathrin-coated pits and caveolae exist, is coated with a filamentous, net-like structure.

The extensive filamentous, net-like structures shown in the magnified images of the cytoplasmic surface of the plasma membrane in Figs. 6A and B, which were

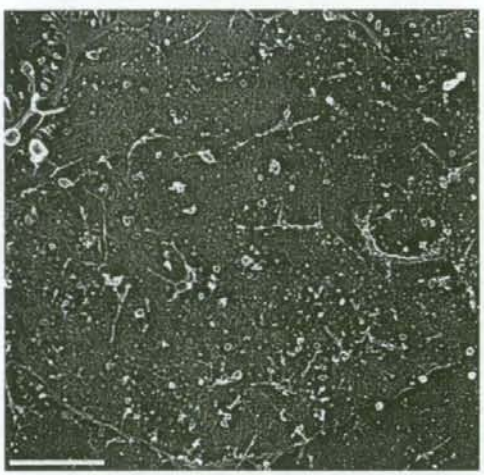

Fig. 5 EM image of the cytoplasmic surface of the upper plasma membrane (bird's-eye view). The plasma membrane fragment shown here represents about a quarter of the upper plasma membrane. Reproduced from Morone *et al.* (2006). © 2003 The Rockfeller University Press.

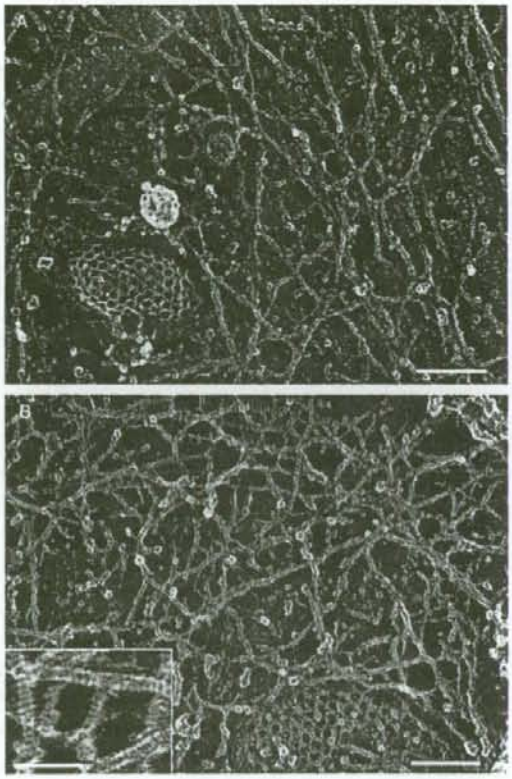

Fig. 6 EM images of the MSK of the upper plasma membrane. (A) NRK cell. (B) FRSK cell. Clathrin-coated structures (A and B) and a caveola (A) show the cytoplasmic surface. The striped banding patterns with the 5.5-nm periodicity on individual filaments are characteristic of actin filaments. These images reveal the close links of the MSK actin filaments with the clathrin-coated structures and caveolae. Bars = 100 nm. The bar in the inset in B = 50 nm. Reproduced from Morone *et al.* (2006).

obtained for an NRK cell (A) and an FRSK cell (B), respectively, are the MSK. The presence of clathrin-coated structures shows that this is indeed the cytoplasmic surface. The striped banding patterns with a 5.5-nm periodicity on individual filaments are characteristic of actin filaments, and thus indicate that these are actin filaments (Heuser and Kirschner, 1980; Katayama, 1998; Schoenenberger *et al.*, 1999). Since almost all of these filaments contain this striped pattern, it was thus concluded that *the MSK is predominantly composed of actin filaments*. This was also confirmed by immunogold staining.

The inset in Fig. 6B indicates the spatial resolution: since each band in the striped pattern with a 5.5-nm periodicity is visibly separated, the effective resolution is thought to be $\approx$ 2 nm (both the thickness of the platinum coating and the platinum granule size are $\leq$ 2 nm: Heuser and Kirschner, 1980; Heuser, 1983).

The MSK structure observed here on the upper cell membrane is similar to that on the bottom cell membrane (the part of the cell membrane facing the coverslip) observed previously (Heuser and Anderson, 1989). Based on these observations, it was concluded that the entire cytoplasmic surface of the plasma membrane is coated with the filamentous actin network (MSK), except for the places where clathrin-coated pits and caveolae are present. The notion of the complete coverage of the cytoplasmic surface of the plasma membrane by actin filaments might have existed for over 30 years in part of the EM community (Byers and Porter, 1977; see Sheetz *et al.*, (2006) for a review), but the data specifically indicating that the actin filaments of the MSK may cover the entire plasma membrane had neither been presented in the literature, as done by Morone *et al.* (2006), nor shared in the cell biology community. The EM observations described here are consistent with the MSK-fence and anchored transmembrane protein picket models, in which the entire plasma membrane, except for specific membrane domains, is parceled up into apposed domains, with regard to the lateral diffusion of the molecules incorporated in the plasma membrane (Fujiwara *et al.*, 2002; Kusumi *et al.*, 2005a,b).

B. View of the MSK Using Anaglyphs

A representative anaglyph produced from images taken at $\pm 12°$ is shown in Fig. 7. In these images, because of their 3D representation, it is especially clear that the MSK, which is mostly composed of actin filaments, generally spreads along the plasma membrane, covering almost the entire cytoplasmic surface of the upper plasma membrane. In addition, clathrin-coated pits and caveolae are very closely associated with the actin filaments in the MSK, as seen in this image as well as in Figs. 6A and B. These results are consistent with those reported by Fujimoto *et al.* (2000), Rothberg *et al.* (1992), and Parton, (2003), but in the NRK cells studied here, 92 and 93% of clathrin-coated pits and caveolae ($n = 200$) are bound by the actin filaments. Furthermore, in these images, many actin filaments are associated with each clathrin-coated pit or caveola. These results are consistent with the requirement of f-actin for clathrin-coated pit internalization (cf. Merrifield *et al.*, 2002; Qualmann *et al.*, 2000).

Many short, thin filaments protrude toward the cytoplasm, mostly perpendicularly, from the membrane surface (arrows in Fig. 7; they were short probably because they were broken when the membrane was ripped off). Note that these perpendicular filaments are almost always connected to the MSK network lying on the cytoplasmic surface (see the tips of the arrows). Thus, the part of the MSK that is located on the cytoplasmic surface is connected three-dimensionally to

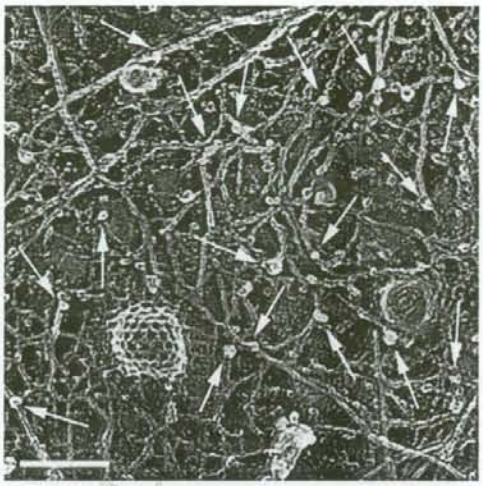

Fig. 7 Stereo electron micrograph (anaglyphs; left = red, right = green) of the plasma membrane undercoat structure generated at ±12° of the tilt angle among the 131 tilt images (acquired in the range of ±65° with 1° steps). For the 3D view, one will need red-blue viewing glasses. These glasses are widely available online or via novelty sources, such as comic book shops and toy stores, and are often attached to Journals [for example, J. Cell Biol. 2006 vol.174, No.6)] or confocal microscopes. We will send a pair upon request at singlemolecules111<at>frontier.kyoto-u.ac.jp. Arrows: actin filaments protruding from the membrane cytoplasmic surface toward the cytoplasm. The arrows point to the places where the protruding actin filaments intersect with the actin filaments lying horizontally on the plasma membrane. Bar = 100 nm. Reproduced from Morone *et al.* (2006). © 2003 The Rockfeller University Press. (See Color Plate no. 5 in the Color Plate Section.)

the cytoskeleton. Together, they will provide the mechanical support for the membrane and the force for deforming the membrane.

C. Quantitative 3D Reconstruction of the Undercoat Structure on the Cytoplasmic Surface of the Plasma Membrane Using Electron Tomography

The 3D structure of the undercoat within 100–134 nm from the cytoplasmic surface of the plasma membrane, which includes clathrin-coated pits, caveolae, and the actin-based MSK, was reconstructed using electron tomography for the platinum replicated samples. Based on the 97–141 tilt images acquired in the range of ±48–70° every 1° step for a single EM view field, 100–121 sliced images of every 0.85–1.34 nm perpendicular to the z-axis (parallel to the image obtained at 0° of the tilt angle) were calculated by a computer (long-wavelength [≥~500 nm] undulations of the cell membrane were corrected by the 3D-reconstruction software, IMOD). The 3D-image was reconstructed based on these serial thin slices.

In Fig. 8A, a typical MSK structure quantitatively analyzed in the present work is shown in an anaglyph, and its 8.5-nm thick sections (created by superimposing ten 0.85-nm sections) of the MSK of an NRK cell, starting from the cytoplasmic side toward the membrane, are shown (Fig. 8B). The actin-based MSK is visible on image sections 81 through 110. Individual actin filaments, forming a network as well as bundles, can be identified. Given the high density of the actin filament meshwork, which is much smaller than the optical resolution, conventional fluorescence microscopy cannot be used to observe the individual actin filaments, and can visualize only the bundles of actin filaments.

D. Interface Structure of the MSK on the Cytoplasmic Surface of the Plasma Membrane

The part of the actin-based MSK that contacts the cytoplasmic surface of the plasma membrane has been proposed to partition the cell membrane into 30–230 nm compartments, by the "fence and picket" effect (Edidin *et al.*, 1991; Kusumi and Sako, 1996; Kusumi *et al.*, 2005a,b), for the diffusion of membrane molecules. If these fence and picket models are correct, then the distribution of the mesh size of the MSK on the cytoplasmic surface of the plasma membrane would be practically the same as that of the compartment size determined by diffusion measurements of membrane molecules. To carry out this examination, the 3D reconstruction of the MSK by electron tomography provides a unique opportunity, because the obtained images provide quantitative data on the distance between the individual filaments and the membrane surface.

The actin filaments of the MSK that are directly associated with the cytoplasmic surface of the plasma membrane and may be involved in partitioning the plasma membrane were systematically determined. Out of the stack of 121 image slices taken every 0.85 nm from the cytoplasmic surface ($\approx$ 100-nm thick altogether), 16 consecutive image slices from the membrane surface ($\approx$ 13.6-nm thick altogether) were used for this analysis (Figs. 9A and B).

In Figs. 9A (four images on the right) and 9B (from the second to the fourth images), the square boxes in the left-most images were expanded, and the sections of every 1.7 nm (superposition of two 0.85-nm-thick slices, 330 $\times$ 330 nm) are displayed, between 0 and 11.9 nm. Using these sections, the filaments that are closely associated with the cytoplasmic surface of the cell membrane were determined. Since the width of the actin filament after platinum shadowing is between 9–11 nm (consistent with Heuser, 1983) and the thickness of the platinum replica is $\leq$ 2 nm (consistent with Heuser, 1983 and Moritz *et al.*, 2000), the height of the actin filament that is associated with the membrane will be 7–9 nm (because the height is given by the actin thickness and one replica thickness, whereas the width of the actin filament in the image is determined by the actin thickness plus two replica thicknesses), with 8 nm being a reasonable estimate.

The electron tomography sections shown in Figs. 9A and B revealed three major classes of filaments, with regard to the distance from the membrane surface.

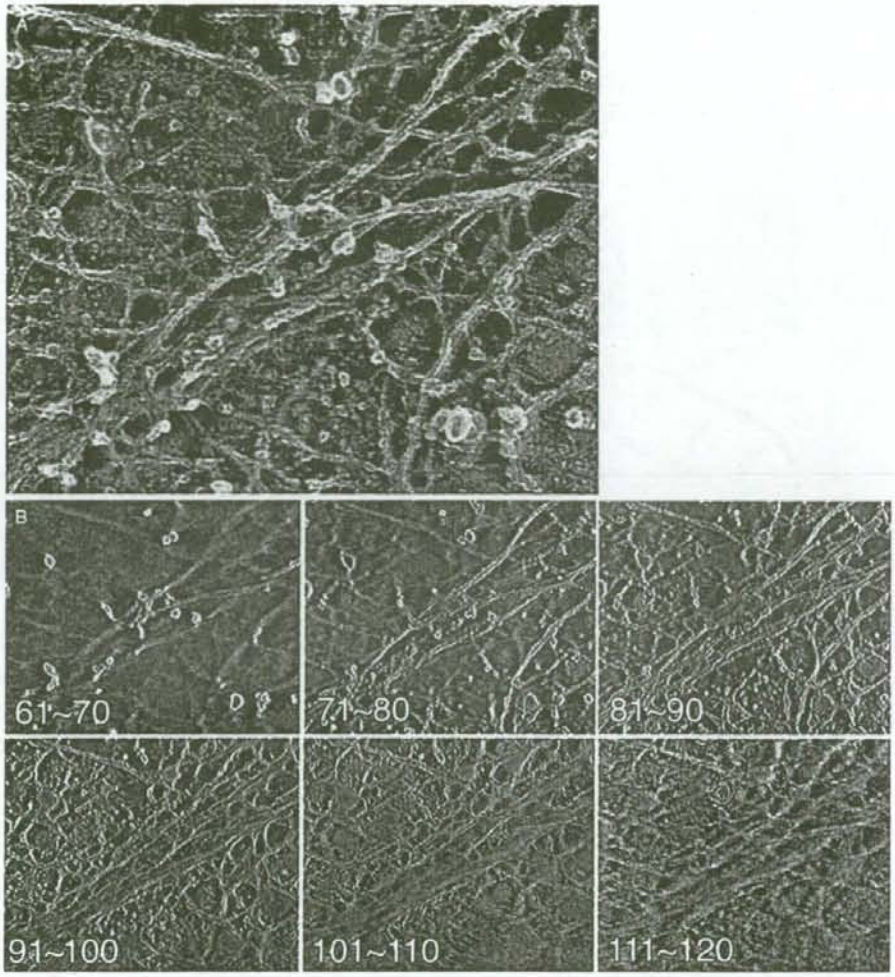

Fig. 8 A typical actin MSK structure on the cytoplasmic surface of the plasma membrane of an NRK cell. (A) An anaglyph of a typical actin MSK structure generated at ±12° of the tilt angle among the 97 tilt images (acquired in the range of ±48° with 1° steps). (B) A typical series of sliced images of the actin MSK. Ten consecutive sections, each 0.85-nm thick, are superimposed, and six of these superimposed images, representing 60 image sections out of 121 image sections, are shown from the cytoplasmic side toward the plasma membrane side. The numbers here indicate the number of slices counted from the cytoplasmic side. The actin-based MSK near the cytoplasmic surface of the plasma membrane is visible on images 81 through 110. Reproduced from Morone *et al.* (2006). © 2003 The Rockfeller University Press. (See Color Plate no. 6 in the Color Plate Section.)

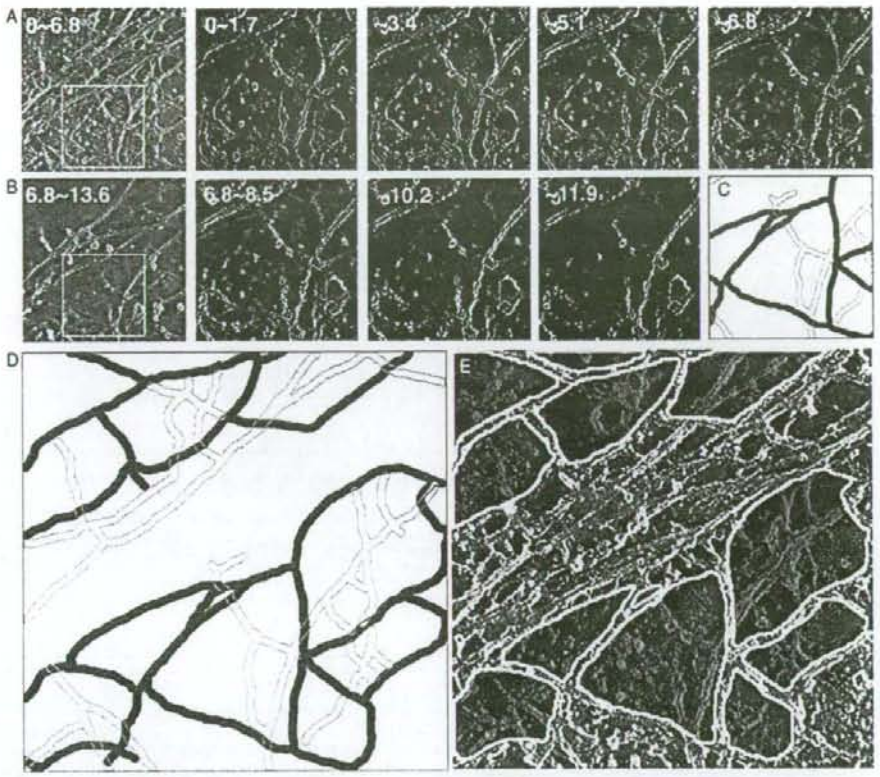

Fig. 9 The method for determining the MSK mesh on the cytoplasmic surface of the plasma membrane, which possibly delimits the compartments of the plasma membrane, using the 3D-reconstructed images of the MSK (an NRK cell). (A, B) The images on the far left are the 0 ~ 6.8 nm or 6.8 ~ 13.6 nm sections, each of which is a stack of eight 0.85-nm sections of 670 × 670 nm. These are from a series of 121 image sections (0.85-nm thick) from the cytoplasmic surface, after the tilt and the long-wavelength undulation of the cell surface were corrected. The images in the white squares in (A) and (B) (330 × 330 nm) are expanded on the right of these image stacks, with a section thickness of 1.7 nm (two 0.85-nm sections are superimposed)(330 × 330 nm for each image). (C) The outline of each actin filament adjacent to the membrane surface (green, which could not be observed above 10.2 nm) and that of each actin filament that could be observed above 10.2 nm (red). The view field and magnification are the same as those for the thinner sections shown in (A) and (B) (330 × 330 nm). See the Methods section for details. (D) The outline of actin filaments in a greater view field, which is the same as those in the thick sections (0 ~ 6.8 nm and 6.8 ~ 13.6 nm) in (A) and (B) (670 × 670 nm, expanded here). (E) The image of the 0 ~ 6.8 nm sections (670 × 670 nm), superimposed on the image of the areas surrounded by the filaments outlined in green in (D) (green areas with yellow outlines). According to the "fence" and "picket" models, these areas are likely to be the compartments where the membrane molecules are temporarily confined. Reproduced from Morone *et al.* (2006). © 2003 The Rockfeller University Press. (See Color Plate no. 7 in the Color Plate Section.)

The actin filaments of the first class are distinct even in the first 0 ~ 1.7 nm section (since the contrast is reversed in these micrographs, they look more lucent or white), but they fade out of the reconstructions 8–10 nm away from the membrane surface. These filaments are drawn in green in Fig. 9C. We interpreted this to mean that these filaments are in close contact with the plasma membrane, with the gap between the filament and the inner membrane surface being less than 0.85 nm, because they can be seen clearly even in the first 0.85-nm section. These filaments are likely to be the significant ones for generating membrane corrals (for more quantitative analyses and descriptions, see Morone *et al.*, (2006)).

The filaments of the second class are also clearly visible in the sections very close to the membrane surface, but they do not fade out until about 14 nm away from the surface. These are probably the actin filaments that caught the platinum coating all around their surfaces because they resided slightly off the surface. The extra coating slightly exaggerated their thickness and made them look as though they were in contact with the plasma membrane, when in fact they probably were not quite in direct contact. We did *not* consider these filaments to be close enough to generate membrane corrals.

The actin filaments of the third class are not apparent in the sections closest to the plasma membrane, but they become clear some distance away from it (greater than 2–4 nm), and they also do not fade out until ~14 nm. We interpreted this to mean that these filaments are those that definitely do not contact the plasma membrane directly, and hence should not contribute to forming corrals. The second and third classes of filaments are drawn in red in Fig. 9C.

Therefore, we considered that only the first class of filaments (those drawn in green in Figs. 9C and D) forms the MSK fences and pickets, and the area surrounded by these filaments is colored green in the 0–6.8 nm section shown in Fig. 9E. Note that there are regions that were not amenable to such an analysis. They were the areas where the bundles of actin filaments are present (e.g., the structure crossing diagonally from the lower left to the upper right in Fig. 8), the actin filaments are too crowded to be individually discerned, the actin filament is terminated in the middle of a domain (domains that contain a loose end of an actin filament) or the clathrin-coated pits, caveolae, and the smooth-surface membrane invaginations are present. They were excluded from this analysis (the white regions in Fig. 10C).

E. Distribution of the MSK Mesh Size on the Plasma Membrane Determined by Electron Tomography

A similar determination of the MSK meshwork was also made for FRSK cells. Representative meshes of the MSK are shown in Fig. 10 (for an FRSK cell, colored to aid visualization). We carried out such analyses for 10 representative stacks of image sections (1290 nm × 1290 nm plane) each for NRK cells and FRSK cells (eight different cell membrane sheets for each cell type), and identified 76 and 1300 areas bounded by the MSK meshwork, respectively. The two-dimensional area size

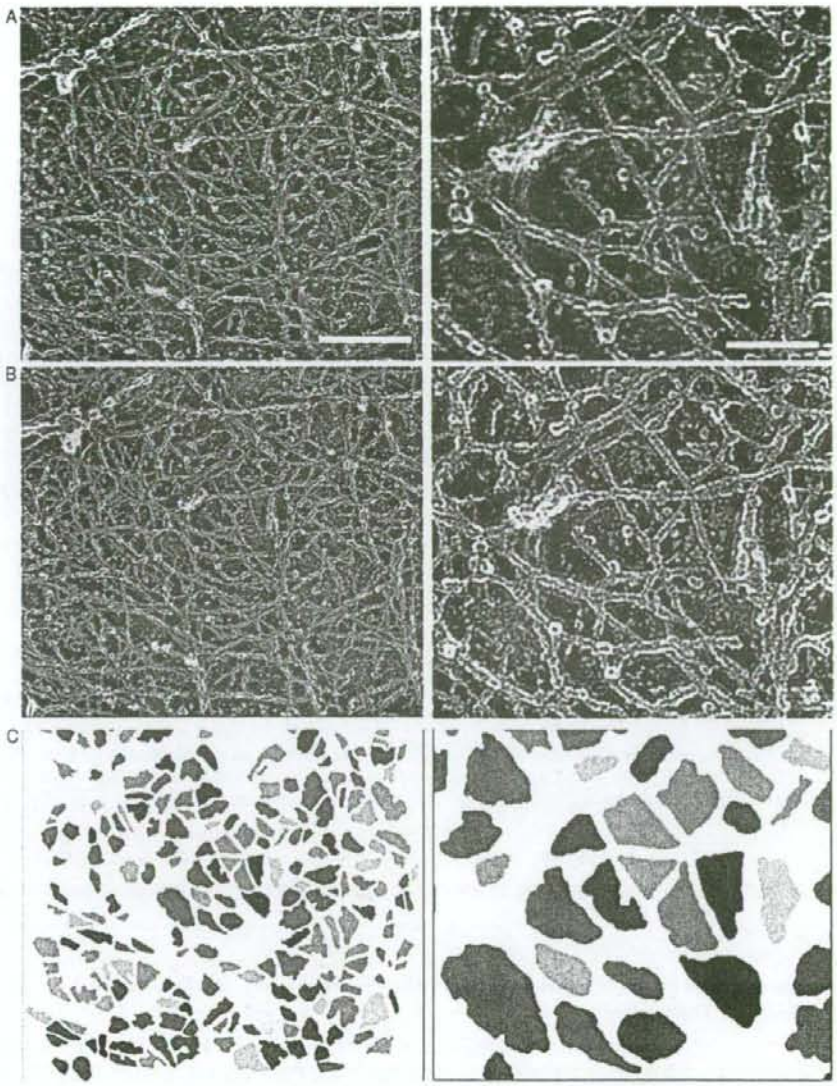

Fig. 10 The MSK meshwork directly located on the cytoplasmic surface of the plasma membrane of an FRSK cell. The central parts of the figures in the left column (bar = 300 nm) are magnified by a factor of 3, and are shown in the right column (bar = 100 nm). (Row A) Typical stereo views of the plasma membrane specimen (anaglyph; left = red, right = green). (Row B) Normal electron

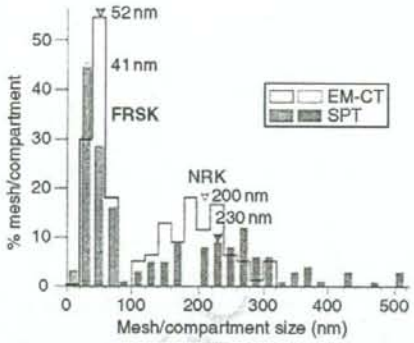

Fig. 11 Comparison of the distributions of the MSK mesh size on the cytoplasmic surface of the plasma membrane estimated by electron tomography (open bars), with that of the compartment size determined from the phospholipid diffusion data (closed bars, adapted from Fujiwara *et al.* (2002) and Murase *et al.* (2004)), for NRK (magenta) and FRSK (blue) cells. Within the same cell type, the MSK mesh size and the diffusion compartment size exhibited similar distributions (compare the open and closed bars with the same color). The actual sizes are quite different between NRK and FRSK cells. Reproduced from Morone *et al.* (2006). © 2003 The Rockfeller University Press.

for each domain was measured by the AMIRA software. The distributions of the square root of the area size (the side length, assuming a square shape for the area) for NRK (magenta open bars) and FRSK (blue open bars) cells are shown in Fig. 11. The median values of the area and its square root are 3.9×10^4 nm^2 and 200 nm, respectively, for NRK cells, and 2.7×10^3 nm^2 and 52 nm, respectively, for FRSK cells.

F. Comparison of the MSK Mesh Size on the Plasma Membrane Determined by Electron Tomography with the Compartment Size for Membrane Molecule Diffusion

Our group has proposed that a part of the MSK is directly and closely associated with the cytoplasmic surface of the plasma membrane, and that this close association of parts of the MSK meshwork induces partitioning of the plasma membrane, with regard to the translational diffusion of membrane molecules, based on high speed single-particle tracking data for membrane proteins and lipids (Fig. 12, Jacobson *et al.*, 1995; Kusumi and Sako, 1996; Kusumi *et al.*, 2005b). Namely, the entire plasma membrane is parceled up into apposed domains by the MSK meshwork associated with the plasma membrane. In the short-time regime, these

micrographs of the plasma membrane samples. The same view fields as those in A. (Row C) The areas delimited by the actin filaments closely apposed to the cytoplasmic surface of the cell membrane are shown. Different colors are used to aid in visualization. Reproduced from Morone *et al.* (2006). © 2003 The Rockfeller University Press. (See Color Plate no. 8 in the Color Plate Section.)

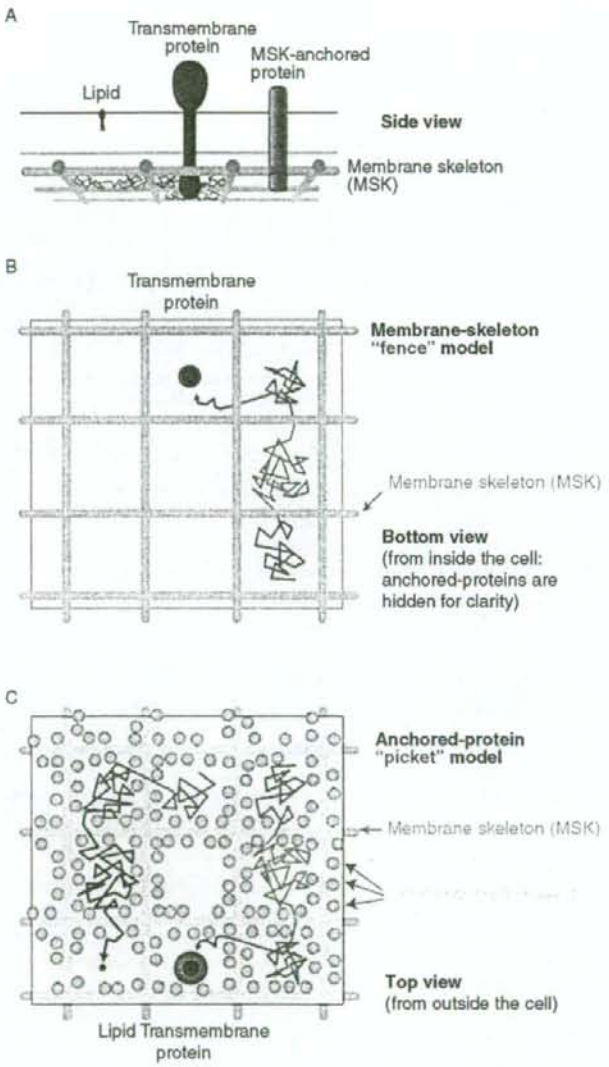

Fig. 12 Proposed mechanisms for the compartmentalization of the plasma membrane for the translational diffusion of transmembrane proteins and phospholipids (located in the *outer* leaflet) in the membrane: Corralling by the membrane-skeleton "fences" and the anchored-protein "pickets". The plasma membrane may be parceled up into closely apposed domains (compartments) for the translational diffusion of transmembrane proteins and lipids (even those located in the outer leaflet).

membrane molecules are temporarily confined within the compartments delimited by the MSK mesh, and, in the long-time regime, they undergo macroscopic diffusion by hopping between these compartments. The Singer-Nicolson model of the membrane is only suitable for a description of diffusion on the scale of ~10 nm in the plasma membrane, but the presence of such compartment boundaries must be considered for the diffusion over distances of several 10 s of nanometers.

Transmembrane proteins are temporarily confined within a compartment, due to the collision of their cytoplasmic domains with the actin filaments in the MSK mesh, closely located on the surface of the plasma membrane (MSK-"fence" model, Fig. 12; also see Sako and Kusumi, 1995; Sako *et al.*,1998; Suzuki *et al.*, 2005; Tomishige *et al.*, 1998).

Lipid molecules also undergo hop diffusion, which might be explained by the "anchored-protein picket model" (Fujiwara *et al.*, 2002; Kusumi *et al.*, 2005b; Murase *et al.*, 2004). In this "picket" model, various transmembrane proteins anchored to and aligned along the actin filaments that are located right on the cytoplasmic surface of the plasma membrane might effectively act as rows of pickets against the free diffusion of all of the molecules incorporated in the cell membrane. This is due to the steric hindrance and circumferential slowing of the immobile picket proteins, anchored to and lined up along the MSK. Here, the circumferential slowing due to the hydrodynamic friction-like effect of the immobile picket proteins (Bussell *et al.*, 1995a,b) is critical for effectively blocking the passage of membrane molecules across the picket line, because this effect will propagate quite far from the immobile protein surface. Without this effect, the picket model would not be valid. Lipid movement is affected only by pickets, whereas both pickets and fences would act on transmembrane proteins.

The size distributions of the compartments for the diffusion of membrane molecules were obtained for an unsaturated phospholipid, L-α-dioleoylphosphatidylethanolamine, by Fujiwara *et al.* (2002) and Murase *et al.* (2004), for NRK and FRSK cells, respectively. The distributions of the side lengths for NRK (magenta closed bars) and FRSK (blue closed bars) cells are shown in the histograms in Fig. 12. The median values of the compartment area and the side length are 4.3×10^4 nm^2 and 230 nm, respectively, for NRK cells, and 2.1×10^3 nm^2 and 41 nm, respectively, for FRSK cells (Murase *et al.*, 2004).

All of the membrane constituent molecules undergo short-term confined diffusion within a compartment and long-term hop diffusion between these compartments. This may be due to corralling by two mechanisms: The membrane-skeleton "fences" and the anchored-protein "pickets". (A) Side-view schematic representation of a transmembrane protein, a phospholipid located in the outer leaflet, and an MSK-anchored protein (membrane skeleton-anchored protein, grey cylinder). The former two molecules are mobile, whereas the MSK-anchored protein is immobile. (B) The membrane-skeleton "fence" or "corral" model, showing that transmembrane proteins are confined within the mesh of the actin-based membrane skeleton, as viewed from inside the cell. Meanwhile the phospholipids located in the outer leaflet of the membrane do not directly interact with the membrane skeleton. (C) The anchored-protein "picket" model, showing the MSK-anchored proteins effectively represent immobile obstacles to the diffusion of transmembrane proteins and phospholipids, as viewed from outside the cell. (See Color Plate no. 9 in the Color Plate Section.)

These results indicate that in the same cell line (for both the NRK and FRSK cases), the MSK mesh size determined by electron tomography and the diffusion compartment size determined by the high-speed single-particle tracking of a phospholipid are similar to each other. However, between these two cell lines, both the MSK mesh and the diffusion compartment sizes differ greatly. The similarities between the MSK mesh sizes and the diffusion compartment sizes in cell lines that exhibit quite different distributions strongly support the MSK fence and picket models.

IV. Electron Tomography Clarified that Some of the Actin Filaments are Laterally Bound to the Cytoplasmic Surface of the Plasma Membrane

Many mammalian cells have a well-developed cytoskeleton in the bulk cytoplasm. The cytoskeleton consists of actin filaments, intermediate filaments, such as keratin filaments and neurofilaments, and microtubules. Since actin filaments are more involved in cell movement and morphological changes of the cell than the others, they have been believed to be associated with the plasma membrane, at least in the regions of leading edges and membrane ruffles. However, since the interactions of the actin filaments with the plasma membrane have traditionally been investigated in this context, in the actin literature, researchers have almost always assumed that, to understand their interactions, it is sufficient to consider that the barbed-ends of the actin filaments are bound to the plasma membrane, and that they can neglect the lateral binding of the actin filaments to the components of the plasma membrane.

In the late 1980s, actin binding and nucleation on the cytoplasmic surface of the plasma membrane were investigated (Schwartz and Luna, 1986, 1988; Tranter *et al.*, 1989), and ponticulin, a transmembrane protein in the Dictyostelium discoideum plasma membrane that laterally binds to actin filaments, was discovered (Wuestehube and Luna, 1987). Since then, biochemical analyses have revealed many more proteins that exhibit lateral binding to the actin filaments as well as binding to membranes and membrane molecules. These proteins include the Ezrin/Radixin/Moesin (ERM)-family of proteins (Hamada *et al.*, 2003; James *et al.*, 2001), the villin-gelsolin-superfamily proteins including fimbrin and supervillin (Pestonjamasp *et al.*, 1997, where the involvement of supervillin in adhesion structures is described), Epithelial protein lost in neoplasm (EPLIN), which binds to the cadherin-catenin complex (Abe and Takeichi, 2008; Maul *et al.*, 2003), filamin, which is involved in various membrane-protein functions (Stossel *et al.*, 2001; Tavano *et al.*, 2006; Uribe and Jay, 2007), dystrophin and utrophin, which, like tropomyosin, are likely to bind to actin filaments (Fig. 1; Rybakova and Ervasti, 1997; Rybakova *et al.*, 2002), and, let us not forget the myosin-family of proteins, including myosin-I. Namely, *these proteins are likely to mediate the lateral binding of*

actin filaments to the cytoplasmic surface of the plasma membrane, and thus *lateral binding as well as barbed-end binding* is important for understanding the MSK functions and the interaction between the plasma membrane and the cytoskeleton.

However, very few systematic structural studies of the MSK at the interface with the plasma membrane have been carried out. The actin filaments laterally bound to the plasma membrane have not received sufficient attention, despite their possibly important functions. This is partly due to the technical difficulties in obtaining large plasma membrane specimens that allow high resolution observations, without introducing too many artifacts. We think that 3D reconstructions of the MSK, using electron tomography with frozen-etched, platinum-replicated plasma membrane specimens, may be ideal for carrying out ultrastructural observations of the interface between the MSK and the plasma membrane. We hope that this review enhances the readers' interests in the interface structures between the MSK and the plasma membrane, and that the methods described in this review will help the readers to perform electron microscopic as well as tomographic studies of the interactions of the MSK with the plasma membrane.

Acknowledgments

We would like to thank Shigeki Yuasa and John Heuser for their helpful advice and encouragement throughout this electron tomography work. This work was supported in part by World Premier International Research Center Initiative (WPI initiative) of the Ministry of Education, Culture, Sports, Science, and Technology (MEXT) of the Japanese government, and also by Health Labor Sciences Research Grant nano-001 to N. Morone, and Grants-in-Aid for Scientific Research and that on Priority Areas from the MEXT to J. Usukura and A. Kusumi.

References

Abe, K., and Takeichi, M. (2008). EPLIN mediates linkage of the cadherin catenin complex to F-actin and stabilizes the circumferential actin belt. *Proc. Natl. Acad. Sci. USA* **105,** 13–19.

Bennett, V. (1990). Spectrin-based membrane skeleton: A multipotential adaptor between plasma membrane and cytoplasm. *Physiol. Rev.* **70,** 1029–1065.

Bussell, S. J., Koch, D. L., and Hammer, D. A. (1995a). Effect of hydrodynamic interactions on the diffusion of integral membrane proteins: Tracer diffusion in organelle and reconstituted membranes. *Biophys. J.* **68,** 1828–1835.

Bussell, S. J., Koch, D. L., and Hammer, D. A. (1995b). Effect of hydrodynamic interactions on the diffusion of integral membrane proteins: Diffusion in plasma membranes. *Biophys. J.* **68,** 1836–1849.

Byers, H. R., and Porter, K. R. (1977). Transformations in the structure of the cytoplasmic ground substance in erythrophores during pigment aggregation and dispersion. I. A study using whole-cell preparations in stereo high voltage electron microscopy. *J. Cell Biol.* **75,** 541–558.

Byers, T. J., and Branton, D. (1985). Visualization of the protein associations in the erythrocyte membrane skeleton. *Proc. Natl. Acad. Sci. USA* **82,** 6153–6157.

Chandler, D. E., and Heuser, J. (1979). Membrane fusion during secretion: Cortical granule exocytosis in sex urchin eggs as studied by quick-freezing and freeze-fracture. *J. Cell Biol.* **83,** 91–108.

Choquet, D., Felsenfeld, D. P., and Sheetz, M. P. (1997). Extracellular matrix rigidity causes strengthening of integrin-cytoskeleton linkages. *Cell* **88,** 39–48.

Coleman, T. R., Fishkind, D. J., Mooseker, M. S., and Morrow, J. S. (1989). Functional diversity among spectrin isoforms. *Cell Motil. Cytoskeleton* **12,** 225–247.

Edidin, M., Kuo, S. C., and Sheetz, M. P. (1991). Lateral movements of membrane glycoproteins restricted by dynamic cytoplasmic barriers. *Science* **254,** 1379–1382.

Evans, E. A. (1989). Structure and deformation properties of red blood cells: Concepts and quantitative methods. *Meth. Enzymol.* **173,** 3–35.

Fujimoto, K. (1995). Freeze-fracture replica electron microscopy combined with SDS digestion for cytochemical labeling of integral membrane proteins. Application to the immunogold labeling of intercellular junctional complexes. *J. Cell Sci.* **108**(Pt 11), 3443–3449.

Fujimoto, K., Umeda, M., and Fujimoto, T. (1996). Transmembrane phospholipid distribution revealed by freeze-fracture replica labeling. *J. Cell Sci.* **109**(Pt 10), 2453–2460.

Fujimoto, L. M., Roth, R., Heuser, J. E., and Schmid, S. L. (2000). Actin assembly plays a variable, but not obligatory role in receptor-mediated endocytosis in mammalian cells. *Traffic* **1,** 161–171.

Fujita, A., Cheng, J., Hirakawa, M., Furukawa, K., Kusunoki, S., and Fujimoto, T. (2007). Gangliosides GM1 and GM3 in the living cell membrane form clusters susceptible to cholesterol depletion and chilling. *Mol. Biol. Cell* **18,** 2112–2122.

Fujiwara, T., Ritchie, K., Murakoshi, H., Jacobson, K., and Kusumi, A. (2002). Phospholipids undergo hop diffusion in compartmentalized cell membrane. *J. Cell Biol.* **157,** 1071–1081.

Hainfeld, J. F., and Steck, T. L. (1977). The sub-membrane reticulum of the human erythrocyte: A scanning electron microscope study. *J. Supramol. Struct.* **6,** 301–311.

Hamada, K., Shimizu, T., Yonemura, S., Tsukita, S., and Hakoshima, T. (2003). Structural basis of adhesion-molecule recognition by ERM proteins revealed by the crystal structure of the radixin-ICAM-2 complex. *EMBO J.* **22,** 502–514.

Hanson, P. I., Roth, R., Lin, Y., and Heuser, J. E. (2008). Plasma membrane deformation by circular arrays of ESCRT-III protein filaments. *J. Cell Biol.* **180,** 389–402.

Hanson, P. I., Roth, R., Morisaki, H., Jahn, R., and Heuser, J. E. (1997). Structure and conformational changes in NSF and its membrane receptor complexes visualized by quick-freeze/deep-etch electron microscopy. *Cell* **90,** 523–535.

Hartwig, J. H., Chambers, K. A., and Stossel, T. P. (1989). Association of gelsolin with actin filaments and cell membranes of macrophages and platelets. *J. Cell Biol.* **108,** 467–479.

Heuser, J. (2005). Deep-etch EM reveals that the early poxvirus envelope is a single membrane bilayer stabilized by a geodetic "honeycomb" surface coat. *J. Cell Biol.* **169,** 269–283.

Heuser, J. E. (1983). Procedure for freeze-drying molecules adsorbed to mica flakes. *J. Mol. Biol.* **169,** 155–195.

Heuser, J. E. (2000). Membrane traffic in anaglyph stereo. *Traffic* **1,** 35–37.

Heuser, J. E., and Anderson, R. G. (1989). Hypertonic media inhibit receptor-mediated endocytosis by blocking clathrin-coated pit formation. *J. Cell Biol.* **108,** 389–400.

Heuser, J. E., and Kirschner, M. W. (1980). Filament organization revealed in platinum replicas of freeze-dried cytoskeletons. *J. Cell Biol.* **86,** 212–234.

Heuser, J. E., Reese, T. S., Dennis, M. J., Jan, Y., Jan, L., and Evans, L. (1979). Synaptic vesicle exocytosis captured by quick freezing and correlated with quantal transmitter release. *J. Cell Biol.* **81,** 275–300.

Hirokawa, N., and Heuser, J. E. (1981). Quick-freeze, deep-etch visualization of the cytoskeleton beneath surface differentiations of intestinal epithelial cells. *J. Cell Biol.* **91,** 399–409.

Hirokawa, N., Tilney, L. G., Fujiwara, K., and Heuser, J. E. (1982). Organization of actin, myosin, and intermediate filaments in the brush border of intestinal epithelial cells. *J. Cell Biol.* **94,** 425–443.

Italiano, J. E., Jr., Lecine, P., Shivdasani, R. A., and Hartwig, J. H. (1999). Blood platelets are assembled principally at the ends of proplatelet processes produced by differentiated megakaryocytes. *J. Cell Biol.* **147,** 1299–1312.

Jacobson, K., Sheets, E. D., and Simson, R. (1995). Revisiting the fluid mosaic model of membranes. *Science* **268,** 1441–1442.

James, M. F., Manchanda, N., Gonzalez-Agosti, C., Hartwig, J. H., and Ramesh, V. (2001). The neurofibromatosis 2 protein product merlin selectively binds F-actin but not G-actin, and stabilizes the filaments through a lateral association. *Biochem. J.* **356,** 377–386.

Kajimura, N., Harada, Y., and Usukura, J. (2000). High-resolution freeze-etching replica images of the disk and the plasma membrane surfaces in purified bovine rod outer segments. *J. Electron Microsc. (Tokyo)* **49,** 691–697.

Kanaseki, T., Ikeuchi, Y., and Tashiro, Y. (1998). Rough surfaced smooth endoplasmic reticulum in rat and mouse cerebellar Purkinje cells visualized by quick-freezing techniques. *Cell Struct. Funct.* **23,** 373–387.

Kanaseki, T., Kawasaki, K., Murata, M., Ikeuchi, Y., and Ohnishi, S. (1997). Structural features of membrane fusion between influenza virus and liposome as revealed by quick-freezing electron microscopy. *J. Cell Biol.* **137,** 1041–1056.

Katayama, E. (1998). Quick-freeze deep-etch electron microscopy of the actin-heavy meromyosin complex during the *in vitro* motility assay. *J. Mol. Biol.* **278,** 349–367.

Katayama, E., Shiraishi, T., Oosawa, K., Baba, N., and Aizawa, S. (1996). Geometry of the flagellar motor in the cytoplasmic membrane of *Salmonella typhimurium* as determined by stereo-photogrammetry of quick-freeze deep-etch replica images. *J. Mol. Biol.* **255,** 458–475.

Kremer, J. R., Mastronarde, D. N., and McIntosh, J. R. (1996). Computer visualization of three-dimensional image data using IMOD. *J. Struct. Biol.* **116,** 71–76.

Kusumi, A., Ike, H., Nakada, C., Murase, K., and Fujiwara, T. (2005a). Single-molecule tracking of membrane molecules: Plasma membrane compartmentalization and dynamic assembly of raft-philic signaling molecules. *Semin. Immunol.* **17,** 3–21.

Kusumi, A., Nakada, C., Ritchie, K., Murase, K., Suzuki, K., Murakoshi, H., Kasai, R. S., Kondo, J., and Fujiwara, T. (2005b). Paradigm shift of the plasma membrane concept from the two-dimensional continuum fluid to the partitioned fluid: High-speed single-molecule tracking of membrane molecules. *Annu. Rev. Biophys. Biomol. Struct.* **34,** 351–378.

Kusumi, A., and Sako, Y. (1996). Cell surface organization by the membrane skeleton. *Curr. Opin. Cell Biol.* **8,** 566–574.

Landis, D. M., and Reese, T. S. (1981). Astrocyte membrane structure: Changes after circulatory arrest. *J. Cell Biol.* **88,** 660–663.

Lucic, V., Forster, F., and Baumeister, W. (2005). Structural studies by electron tomography: From cells to molecules. *Annu. Rev. Biochem.* **74,** 833–865.

Maul, R. S., Song, Y., Amann, K. J., Gerbin, S. C., Pollard, T. D., and Chang, D. D. (2003). EPLIN regulates actin dynamics by cross-linking and stabilizing filaments. *J. Cell Biol.* **160,** 399–407.

Medalia, O., Weber, I., Frangakis, A. S., Nicastro, D., Gerisch, G., and Baumeister, W. (2002). Macromolecular architecture in eukaryotic cells visualized by cryoelectron tomography. *Science* **298,** 1209–1213.

Merrifield, C. J., Feldman, M. E., Wan, L., and Almers, W. (2002). Imaging actin and dynamin recruitment during invagination of single clathrin-coated pits. *Nat. Cell Biol.* **4,** 691–698.

Mohandas, N., and Chasis, J. A. (1993). Red blood cell deformability, membrane material properties and shape: Regulation by transmembrane, skeletal and cytosolic proteins and lipids. *Semin. Hematol.* **30,** 171–192.

Moritz, M., Braunfeld, M. B., Guenebaut, V., Heuser, J., and Agard, D. A. (2000). Structure of the gamma-tubulin ring complex: A template for microtubule nucleation. *Nat. Cell Biol.* **2,** 365–370.

Morone, N., Fujiwara, T., Murase, K., Kasai, R. S., Ike, H., Yuasa, S., Usukura, J., and Kusumi, A. (2006). Three-dimensional reconstruction of the membrane skeleton at the plasma membrane interface by electron tomography. *J. Cell Biol.* **174,** 851–862.

Murase, K., Fujiwara, T., Umemura, Y., Suzuki, K., Iino, R., Yamashita, H., Saito, M., Murakoshi, H., Ritchie, K., and Kusumi, A. (2004). Ultrafine membrane compartments for molecular diffusion as revealed by single molecule techniques. *Biophys. J.* **86,** 4075–4093.

Nakata, T., and Hirokawa, N. (1992). Organization of cortical cytoskeleton of cultured chromaffin cells and involvement in secretion as revealed by quick-freeze, deep-etching, and double-label immunoelectron microscopy. *J. Neurosci.* **12,** 2186–2197.

Nermut, M. V. (1981). Visualization of the "membrane skeleton" in human erythrocytes by freeze-etching. *Eur. J. Cell Biol.* **25,** 265–271.

Ohno, S., and Takasu, N. (1989). Three-dimensional studies of cytoskeletal organizations in cultured thyroid cells by quick-freezing and deep-etching method. *J. Electron Microsc. (Tokyo)* **38,** 352–362.

Parton, R. G. (2003). Caveolae—from ultrastructure to molecular mechanisms. *Nat. Rev. Mol. Cell Biol.* **4,** 162–167.

Pestonjamasp, K. N., Pope, R. K., Wulfkuhle, J. D., and Luna, E. J. (1997). Supervillin (p205): A novel membrane-associated, F-actin-binding protein in the villin/gelsolin superfamily. *J. Cell Biol.* **139,** 1255–1269.

Qualmann, B., Kessels, M. M., and Kelly, R. B. (2000). Molecular links between endocytosis and the actin cytoskeleton. *J. Cell Biol.* **150,** F111–F116.

Rothberg, K. G., Heuser, J. E., Donzell, W. C., Ying, Y. S., Glenney, J. R., and Anderson, R. G. (1992). Caveolin, a protein component of caveolae membrane coats. *Cell* **68,** 673–682.

Rutter, G., Bohn, W., Hohenberg, H., and Mannweiler, K. (1988). Demonstration of antigens at both sides of plasma membranes in one coincident electron microscopic image: A double-immunogold replica study of virus-infected cells. *J. Histochem. Cytochem.* **36,** 1015–1021.

Rybakova, I. N., and Ervasti, J. M. (1997). Dystrophin-glycoprotein complex is monomeric and stabilizes actin filaments *in vitro* through a lateral association. *J. Biol. Chem.* **272,** 28771–28778.

Rybakova, I. N., Patel, J. R., Davies, K. E., Yurchenco, P. D., and Ervasti, J. M. (2002). Utrophin binds laterally along actin filaments and can couple costameric actin with sarcolemma when overexpressed in dystrophin-deficient muscle. *Mol. Biol. Cell* **13,** 1512–1521.

Sako, Y., and Kusumi, A. (1995). Barriers for lateral diffusion of transferrin receptor in the plasma membrane as characterized by receptor dragging by laser tweezers: Fence versus tether. *J. Cell Biol.* **129,** 1559–1574.

Sako, Y., Nagafuchi, A., Tsukita, S., Takeichi, M., and Kusumi, A. (1998). Cytoplasmic regulation of the movement of E-cadherin on the free cell surface as studied by optical tweezers and single particle tracking: Corralling and tethering by the membrane skeleton. *J. Cell Biol.* **140,** 1227–1240.

Sanan, D. A., and Anderson, R. G. (1991). Simultaneous visualization of LDL receptor distribution and clathrin lattices on membranes torn from the upper surface of cultured cells. *J. Histochem. Cytochem.* **39,** 1017–1024.

Sawada, Y., Tamada, M., Dubin-Thaler, B. J., Cherniavskaya, O., Sakai, R., Tanaka, S., and Sheetz, M. P. (2006). Force sensing by mechanical extension of the Src family kinase substrate p130Cas. *Cell* **127,** 1015–1026.

Schoenenberger, C. A., Steinmetz, M. O., Stoffler, D., Mandinova, A., and Aebi, U. (1999). Structure, assembly, and dynamics of actin filaments *in situ* and *in vitro*. *Microsc. Res. Tech.* **47,** 38–50.

Schwartz, M. A., and Luna, E. J. (1986). Binding and assembly of actin filaments by plasma membranes from Dictyostelium discoideum. *J. Cell Biol.* **102,** 2067–2075.

Schwartz, M. A., and Luna, E. J. (1988). How actin binds and assembles onto plasma membranes from Dictyostelium discoideum. *J. Cell Biol.* **107,** 201–209.

Sheetz, M. P. (2001). Cell control by membrane-cytoskeleton adhesion. *Nat. Rev. Mol. Cell Biol.* **2,** 392–396.

Sheetz, M. P., and Dai, J. (1996). Modulation of membrane dynamics and cell motility by membrane tension. *Trends Cell Biol.* **6,** 85–89.

Sheetz, M. P., Sable, J. E., and Dobereiner, H. G. (2006). Continuous membrane-cytoskeleton adhesion requires continuous accommodation to lipid and cytoskeleton dynamics. *Annu. Rev. Biophys. Biomol. Struct.* **35,** 417–434.

Stossel, T. P., Condeelis, J., Cooley, L., Hartwig, J. H., Noegel, A., Schleicher, M., and Shapiro, S. S. (2001). Filamins as integrators of cell mechanics and signalling. *Nat. Rev. Mol. Cell Biol.* **2,** 138–145.

Suzuki, K. G., Fujiwara, T. K., Edidin, M., and Kusumi, A. (2007a). Dynamic recruitment of phospholipase C gamma at transiently immobilized GPI-anchored receptor clusters induces IP3-Ca^{2+} signaling: Single-molecule tracking study 2. *J. Cell. Biol.* **177,** 731–742.

Suzuki, K. G., Fujiwara, T. K., Sanematsu, F., Iino, R., Edidin, M., and Kusumi, A. (2007b). GPI-anchored receptor clusters transiently recruit Lyn and G alpha for temporary cluster immobilization and Lyn activation: Single-molecule tracking study 1. *J. Cell Biol.* **177,** 717–730.

Svitkina, T. M., Bulanova, E. A., Chaga, O. Y., Vignjevic, D. M., Kojima, S., Vasiliev, J. M., and Borisy, G. G. (2003). Mechanism of filopodia initiation by reorganization of a dendritic network. *J. Cell Biol.* **160,** 409–421.

Svitkina, T. M., Verkhovsky, A. B., and Borisy, G. G. (1995). Improved procedures for electron microscopic visualization of the cytoskeleton of cultured cells. *J. Struct. Biol.* **115,** 290–303.

Takeuchi, M., Miyamoto, H., Sako, Y., Komizu, H., and Kusumi, A. (1998). Structure of the erythrocyte membrane skeleton as observed by atomic force microscopy. *Biophys. J.* **74,** 2171–2183.

Tavano, R., Contento, R. L., Baranda, S. J., Soligo, M., Tuosto, L., Manes, S., and Viola, A. (2006). CD28 interaction with filamin-A controls lipid raft accumulation at the T-cell immunological synapse. *Nat. Cell Biol.* **8,** 1270–1276.

Tomishige, M., Sako, Y., and Kusumi, A. (1998). Regulation mechanism of the lateral diffusion of band 3 in erythrocyte membranes by the membrane skeleton. *J. Cell Biol.* **142,** 989–1000.

Tranter, M. P., Sugrue, S. P., and Schwartz, M. A. (1989). Evidence for a direct, nucleotide-sensitive interaction between actin and liver cell membranes. *J. Cell Biol.* **109,** 2833–2840.

Tsukita, S., and Ishikawa, H. (1980). Cytoskeletal network underlying the human erythrocyte membrane. Thin-section electron microscopy. *J. Cell Biol.* **85,** 567–576.

Uribe, R., and Jay, D. (2007). A review of actin binding proteins: New perspectives. *Mol. Biol. Rep.*

Ursitti, J. A., Pumplin, D. W., Wade, J. B., and Bloch, R. J. (1991). Ultrastructure of the human erythrocyte cytoskeleton and its attachment to the membrane. *Cell Motil. Cytoskeleton* **19,** 227–243.

Vertessy, B. G., and Steck, T. L. (1989). Elasticity of the human red cell membrane skeleton. Effects of temperature and denaturants. *Biophys. J.* **55,** 255–262.

Wuestehube, L. J., and Luna, E. J. (1987). F-actin binds to the cytoplasmic surface of ponticulin, a 17-kD integral glycoprotein from Dictyostelium discoideum plasma membranes. *J. Cell Biol.* **105,** 1741–1751.

Yin, H. L., and Hartwig, J. H. (1988). The structure of the macrophage actin skeleton. *J. Cell Sci. Suppl.* **9,** 169–184.